General transfer-matrix method for optical multilayer systems with coherent, partially coherent, and incoherent interference

Charalambos C. Katsidis and Dimitrios I. Siapkas

The optical response of coherent thin-film multilayers is often represented with Fresnel coefficients in a 2×2 matrix configuration. Here the usual transfer matrix was modified to a generic form, with the ability to use the absolute squares of the Fresnel coefficients, so as to include incoherent (thick layers) and partially coherent (rough surface or interfaces) reflection and transmission. The method is integrated by use of models for refractive-index depth profiling. The utility of the method is illustrated with various multilayer structures formed by ion implantation into Si, including buried insulating and conducting layers, and multilayers with a thick incoherent layer in an arbitrary position.

OCIS codes: 310.6860, 240.5770, 240.0310, 300.6340, 300.6470, 080.2730.

1. Introduction

The coherent optical reflectance and transmittance of a multilayer structure are readily represented, for normally incident radiation, as a product of matrices,[1–4] the system transfer matrix. This matrix method assumes a multilayer structure composed of optically isotropic and homogeneous layers, with plane and parallel faces. The elements of the system transfer matrix can be written in terms of the complex-amplitude reflection and transmission coefficients r and t of the multilayer structure.

It is often necessary to analyze a system of several layers for materials with one-dimensional inhomogeneity. Ion-implanted materials are used as examples of a multilayer modeling application. In particular, doping profiles are simulated by means of partitioning the implanted area into a set of homogeneous parallel-faced sampling layers.[5–9] The refractive index is constant within each layer but varies in magnitude from layer to layer, thus representing the one-dimensional inhomogeneity. Modeling of multilayer heterostructures[7–13] is similarly illustrated provided that appropriate dispersion models are chosen for the refractive index of the different materials in the structure. The assumption of coherent light propagation, implied by the form of the ordinary system transfer matrix, may lead to narrow (Fabry–Perot) oscillations in the calculated reflectance and transmittance spectra. These oscillations occur when at least one of the layers of the multilayer structure is thick enough (compared with the incident radiation wavelength) and transparent enough to yield multiple coherent reflections. Since in practice interference-destroying effects, such as nonparallel surfaces of the thick film or limited resolution, may exist in the measurements, these narrow oscillations are not usually observable. Either because of phase incoherency within the thick layer or because of the limited resolution of the measurement, an option allowing the suppression of the thick-film oscillatory pattern should thus be included in the model. The source bandwidth, $\Delta\lambda$, is an another factor that affects coherence (coherence length, $L = \lambda^2/n\Delta\lambda$).

In this paper a generic matrix method is developed for replacing the ordinary coherent system transfer matrix and for allowing both coherent and incoherent multiple reflections to be taken into account. A first attempt presented elsewhere,[14] restricted by use of analytical expressions to a thin-solid-film multilayer structure on a single thick backsubstrate, is now completed by means of matrix formulation and generalized to any arbitrary succession of coherent,

The authors are with the Solid State Section, Department of Physics, Aristotle University of Thessaloniki, 54006 Thessaloniki, Greece. C. Katsidis's e-mail address is babiskat@her.forthnet.gr.

Received 27 June 2001; revised manuscript received 14 January 2002.

0003-6935/02/193978-10$15.00/0

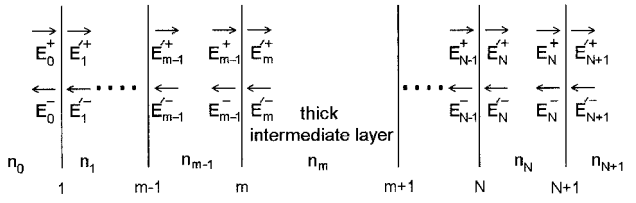

Fig. 1. Notation of electric field amplitudes within an arbitrary multilayer. The subscripts indicate the medium, the + and the − signs distinguish between left- and right-going waves, respectively, whereas a prime is used for waves at the right-hand side of an interface.

incoherent, partially coherent, absorbing, transparent, homogeneous, or inhomogeneous layers. Consequently, analysis of complex structures with absorbing intermediate incoherent layers or with more than one incoherent layer has become feasible. Suppression of interference is achieved in the generic matrix by means of replacing the Fresnel coefficients in the coherent transfer matrix with their absolute squares so that intensities can be added instead of field complex amplitudes. Treating incoherence with the generic matrix yields the same results as do the reflectance and transmittance correction formulas based on partial wave intensity summation, found in literature[15] for an arbitrary thin-solid-film multilayer structure on one side of a thick substrate. In addition, it has the advantage of being applicable to multilayers with a thick layer in an arbitrary position and under certain conditions to multilayers with more than one incoherent layer. The use of the generic matrix is also extended to the conditions of partial coherence. In a previous presentation the convenience of a transfer matrix for incorporating partial coherence was illustrated.[14] Partial coherence, usually resulting from the existence of a rough surface or interface, affects the Fresnel coefficients, which are multiplied by correction factors.[16–19] These modifying factors represent the phase differences in the reflected and the transmitted beams that result from a Gaussian distribution of irregularities. Finally, applications of coherency, partial coherency, and incoherency are illustrated, thus verifying the potential of the generic matrix method for calculating the reflectance and transmittance of any arbitrary succession of thin and thick conducting or insulating layers with rough surfaces and interfaces.

2. Matrix Method

A. Background

The relationship between the tangential components of electric field **E** vector on opposite sides of a film is found to be linear, thus leading to the use of convenient and easy-to-handle matrix equations.

The multilayer structure shown in Fig. 1 is composed of N layers with complex refractive indexes and $N + 1$ interfaces. The subscripts of the field amplitudes in Fig. 1 indicate the medium; the + and − superscripts signify right- and left-going waves, respectively, and the prime is used for waves on the right-hand side of an interface. The use of the + and − superscript electric vectors arises from the description of the tangential electric field, E_t, at any position within the layer as a superposition of two plane waves traversing the medium at opposite directions ($E_t = E_t^+ + E_t^-$).

The field amplitudes in each layer are related by a product of 2×2 matrices in sequence. Each side (for example, i) of an interface is represented by the corresponding dynamical matrix $\mathbf{D}_i$,[3] whereas the action of the bulk of each layer is represented by its propagation matrix, **P**. The field amplitudes on the left-hand side of an interface (for example, E_{m-1}^+ and E_{m-1}^- at the mth interface in Fig. 1) are related with the corresponding field amplitudes on the right-hand side as

$$\begin{pmatrix} E_{m-1}^+ \\ E_{m-1}^- \end{pmatrix} = \mathbf{D}_{m-1}^{-1}\mathbf{D}_m \begin{pmatrix} E_m'^+ \\ E_m'^- \end{pmatrix} = \frac{1}{t_{m-1,m}} \begin{bmatrix} 1 & r_{m-1,m} \\ r_{m-1,m} & 1 \end{bmatrix} \begin{pmatrix} E_m'^+ \\ E_m'^- \end{pmatrix}. \quad (1)$$

The product $\mathbf{D}_{m-1}^{-1}\mathbf{D}_m$ of the dynamical matrices (the so-called refraction or transmission matrix, $\mathbf{D}_{m-1,m}$, of the interface) is a 2×2 matrix, and when expressed in terms of the complex Fresnel reflection, $r_{m-1,m}$, and transmission, $t_{m-1,m}$, coefficients of the interface, it takes the same form in both cases of s or p waves.

The field amplitudes in the left- and the right-hand sides of the $(m - 1)$th layer are related by the propagation matrix $\mathbf{P}_{m-1}$, of the layer:

$$\begin{pmatrix} E_{m-1}'^+ \\ E_{m-1}'^- \end{pmatrix} = \mathbf{P}_{m-1} \begin{pmatrix} E_{m-1}^+ \\ E_{m-1}^- \end{pmatrix} = \begin{bmatrix} \exp(i\delta_{m-1}) & 0 \\ 0 & \exp(-i\delta_{m-1}) \end{bmatrix} \begin{pmatrix} E_{m-1}^+ \\ E_{m-1}^- \end{pmatrix}, \quad (2)$$

where $\delta_{m-1} = 2\pi\sigma n_{m-1} d_{m-1}$ is the phase thickness imposed by the bulk of the $(m - 1)$th layer upon one traversal of light (σ is the wave number and n_{m-1} and d_{m-1} are the refractive index and the thickness of the layer, respectively). The repeated application of the above transformations for the N layers and the $N + 1$ interfaces leads to a product of $N + 1$ 2×2 matrices (one refraction matrix and N layer transfer matrices):

$$\begin{pmatrix} E_0^+ \\ E_0^- \end{pmatrix} = \mathbf{D}_0^{-1} \left[\prod_{m=1}^{N} \mathbf{D}_m \mathbf{P}_m \mathbf{D}_m^{-1} \right] \mathbf{D}_{N+1} \begin{pmatrix} E_{N+1}'^+ \\ E_{N+1}'^- \end{pmatrix} = \begin{bmatrix} T_{11} & T_{12} \\ T_{21} & T_{22} \end{bmatrix} \begin{pmatrix} E_{N+1}'^+ \\ E_{N+1}'^- \end{pmatrix}. \quad (3)$$

The product matrix resulting from the above procedure is again a 2×2 matrix referred to as the system transfer matrix $\mathbf{T} \equiv \mathbf{T}_{0/(N+1)}$.

B. General Matrix Approach: Description of the Method

1. Generalized Form of the Refraction Matrix

The complex reflection and transmission coefficients of the multilayer are given (straightforwardly by

their definitions) in terms of the system transfer matrix elements T_{ij} as

$$r = r_{0,N+1} = \left.\frac{E_0^-}{E_0^+}\right|_{E'^-_{N+1}=0} = \frac{T_{21}}{T_{11}}, \tag{4}$$

$$t = t_{0,N+1} = \left.\frac{E'^+_{N+1}}{E_0^+}\right|_{E'^-_{N+1}=0} = \frac{1}{T_{11}}, \tag{5}$$

$$r' = r_{N+1,0} = \left.\frac{E^-_{N+1}}{E^+_{N+1}}\right|_{E_0^+=0} = -\frac{T_{12}}{T_{11}}, \tag{6}$$

$$t' = t_{N+1,0} = \left.\frac{E_0^-}{E^+_{N+1}}\right|_{E_0^+=0} = \frac{\mathrm{Det}\ T}{T_{11}}$$
$$(\mathrm{Det}\ T = T_{11}T_{22} - T_{12}T_{21}), \tag{7}$$

from which the front and the back reflectances R, R' and transmittances T, T' are obtained as a square of the magnitudes of the complex vectors r, r' and t, t', respectively.

Since Eqs. (4)–(7) relate the T_{ij} elements to the complex reflection and transmission vectors, the T matrix can be written as

$$\mathbf{T}_{0/(N+1)} = \begin{bmatrix} T_{11} & T_{12} \\ T_{21} & T_{22} \end{bmatrix} = \frac{1}{t_{0,N+1}} \begin{bmatrix} 1 & -r_{N+1,0} \\ r_{0,N+1} & t_{0,N+1}t_{N+1,0} - r_{0,N+1}r_{N+1,0} \end{bmatrix}. \tag{8}$$

In this matrix $t_{0,N+1}t_{N+1,0} - r_{0,N+1}r_{N+1,0} = T_{22}/T_{21}$, which generally differs from unity. The application of the above matrix is extended straightforwardly from a multilayer to an interface by means of reducing the reflection and the transmission complex vectors of the multilayer to the corresponding Fresnel coefficients of the interface:

$$\begin{pmatrix} E^+_{m-1} \\ E^-_{m-1} \end{pmatrix} = \frac{1}{t_{m-1,m}} \times \begin{bmatrix} 1 & -r_{m,m-1} \\ r_{m-1,m} & (t_{m-1,m}t_{m,m-1} - r_{m-1,m}r_{m,m-1}) \end{bmatrix} \times \begin{pmatrix} E'^+_m \\ E'^-_m \end{pmatrix}. \tag{9}$$

For nonabsorbing media, the Stokes relations representing the reversibility principle[1] at an ideal interface are $r_{m-1,m} = -r_{m,m-1}$, $t_{m-1,m}t_{m,m-1} - r_{m-1,m}r_{m,m-1} = 1$, and the generalized form reduces to the ordinary refraction matrix. The generalized form of the refraction matrix with $t_{m-1,m}t_{m,m-1} - r_{m-1,m}r_{m,m-1} \neq 1$ can represent either a situation in which the Stokes relations[1] appear to be nonrealistic assumptions of the optical response of an interface (nonideal interface, e.g., a rough one) or just a situation with absorbing media. For absorbing media separated by an ideal interface the Stokes relations take a more general form that contains phase conjugation ($t_{m-1,m}r^*_{m,m-1} + r_{m-1,m}t^*_{m-1,m} = 0$, $t_{m-1,m}t^*_{m,m-1} - r_{m-1,m}r^*_{m-1,m} = 1$) allowing the determinant of the matrix in Eq. (9) to differ from unity.

2. Introduction of Partial Coherence

One can introduce partial coherence produced by macroscopic surface or interface roughness by modifying the Fresnel coefficients of the respective interfaces.[14,16–19] The modifying terms represent the phase differences in the reflected and the transmitted beams that result from a Gaussian distribution of irregularities of height Δh and of rms height Z. The modified coefficients for a rough mth interface ($m = 1$ corresponds to a rough surface) are[14,16,17]

$$r_{m-1,m} = r^{(0)}_{m-1,m} \exp[-2(sn_{m-1}\sigma)^2] = \alpha r^{(0)}_{m-1,m}, \tag{10a}$$

$$r_{m,m-1} = r^{(0)}_{m,m-1} \exp[-2(sn_m\sigma)^2] = \beta r^{(0)}_{m,m-1}, \tag{10b}$$

$$t_{m-1,m} = t^{(0)}_{m-1,m} \exp[-1/2(s\sigma)^2(n_m - n_{m-1})^2] = \gamma t^{(0)}_{m-1,m}, \tag{10c}$$

$$t_{m,m-1} = t^{(0)}_{m,m-1} \exp[-1/2(s\sigma)^2(n_{m-1} - n_m)^2] = \gamma t^{(0)}_{m,m-1}, \tag{10d}$$

where the superscript (0) indicates Fresnel coefficients at smooth interfaces and $s = 2\pi Z$. When working with correlated roughness, one should consider that this approach with correction factors is a scalar treatment.

3. Introduction of Incoherence: Generic Intensity Matrix

Complete incoherence, which usually results from reflection of the beams from the sides of a thick substrate, is treated in a manner more similar to that of coherent reflections than to the partially incoherent ones. No modifying terms such as those in Eqs. (10) are needed, but the squares of the amplitudes of the $\mathbf{r}$, $\mathbf{r}'$, $\mathbf{t}$, and $\mathbf{t}'$ vectors are used instead. Let the mth layer of a multilayer structure composed of N layers and $N + 1$ interfaces be the incoherent one (Fig. 1). The calculation is carried out in two steps. First, the system transfer matrices of the two coherent multilayers are calculated (reducing them to two single effective interfaces bounding the incoherent layer). The complex-amplitude reflection and transmission coefficients of these two multilayer systems are also evaluated from their transfer matrices. When these coefficients are replaced with their square amplitudes, the modified matrices become

$$\mathbf{T}^{\mathrm{int}}_{0/m} = \frac{1}{|t_{0,m}|^2} \begin{bmatrix} 1 & -|r_{m,0}|^2 \\ |r_{0,m}|^2 & (|t_{0,m}t_{m,0}|^2 - |r_{0,m}r_{m,0}|^2) \end{bmatrix}, \tag{11}$$

$$\mathbf{T}^{\mathrm{int}}_{m/(N+1)} = \frac{1}{|t_{m,N+1}|^2} \times \begin{bmatrix} 1 & -|r_{N+1,m}|^2 \\ |r_{m,N+1}|^2 & (|t_{m,N+1}t_{N+1,m}|^2 - |r_{m,N+1}r_{N+1,m}|^2) \end{bmatrix}, \tag{12}$$

and directly yield the reflectance and transmittance of the two coherent multilayers rather than their complex-amplitude reflection and transmission coefficients. These modified matrices (intensity matrices) are then multiplied with the similarly modified propagation matrix of the incoherent mth layer:

$$\mathbf{T}^{\mathrm{int}}_{0/m}\mathbf{P}^{\mathrm{int}}_{m}\mathbf{T}^{\mathrm{int}}_{m/(N+1)} = \frac{1}{|t_{0,m}|^2}\begin{bmatrix} 1 & -|r_{m,0}|^2 \\ |r_{0,m}|^2 & (|t_{0,m}t_{m,0}|^2 - |r_{0,m}r_{m,0}|^2) \end{bmatrix} \times \underbrace{\begin{bmatrix} |\exp(i\delta_m)|^2 & 0 \\ 0 & |\exp(-i\delta_m)|^2 \end{bmatrix}}_{\mathbf{P}^{\mathrm{int}}_{m}} \times \frac{1}{|t_{m,N+1}|^2}\begin{bmatrix} 1 & -|r_{N+1,m}|^2 \\ |r_{m,N+1}|^2 & (|t_{m,N+1}t_{N+1,m}|^2 - |r_{m,N+1}r_{N+1,m}|^2) \end{bmatrix}, \tag{13}$$

to yield the system intensity transfer matrix

$$\mathbf{T}^{\mathrm{incoh}}_{0/(N+1)} = \begin{bmatrix} T^{\mathrm{incoh}}_{11} & T^{\mathrm{incoh}}_{12} \\ T^{\mathrm{incoh}}_{21} & T^{\mathrm{incoh}}_{22} \end{bmatrix} = \mathbf{T}^{\mathrm{int}}_{0/m}\mathbf{P}^{\mathrm{int}}_{m}\mathbf{T}^{\mathrm{int}}_{m/(N+1)}, \tag{14}$$

where $\mathbf{P}^{\mathrm{int}}_{m}$ is the intensity propagation matrix of the incoherent layer (its elements being the square amplitudes of the respective $\mathbf{P}_m$ matrix elements) and reduces to the unity matrix for a transparent layer. In this way, instead of summing the corresponding field amplitudes reflected by the sides of the incoherent layer, we achieve the addition of field intensities as imposed by the complete incoherence.

When $m = N + 1$ in Eq. (14), the general matrix reduces to the coherent intensity matrix $\mathbf{T}^{\mathrm{int}}_{0/(N+1)}$, treating the multilayer as coherent and yielding the reflectivity and the transmissivity rather than their complex amplitudes. When $m = N$ the case of an incoherent finite backsubstrate is encountered, whereas $m < N$ stands for the existence of an intermediate thick incoherent layer.

The reflectance and the transmittance of the system are given by the elements of the incoherent transfer matrix as

$$R_{\mathrm{incoh}} = \frac{T^{\mathrm{incoh}}_{21}}{T^{\mathrm{incoh}}_{11}} = |r_{0,m}|^2 + \frac{|t_{0,m}t_{m,0}r_{m,N+1}|^2 \exp[-4(\sigma/c)k_m d_m)}{1 - |r_{m,0}r_{m,N+1}|^2 \exp[-4(\sigma/c)k_m d_m]}, \tag{15}$$

$$T_{\mathrm{incoh}} = \frac{1}{T^{\mathrm{incoh}}_{11}} = |t_{0,m}|^2 \frac{|t_{m,N+1}|^2 \exp[-2(\sigma/c)k_m d_m]}{1 - |r_{m,0}r_{m,N+1}|^2 \exp[-4(\sigma/c)k_m d_m]}, \tag{16}$$

where media 0 and $N + 1$ are equal and correspond to the medium where the sample is inserted and measured (usually the air). Equations (15) and (16) are in fact the sums of the infinite Airy geometrical series for the field intensities of the partial waves reflected inside the substrate,[15] as expected.

When the finite-thickness substrate is coherent, it is expected that instead of adding field intensities of the partial waves, which are multiply reflected within the thick substrate, we should add the corresponding complex amplitudes. The coherent response of the finite substrate is represented by the generic transfer matrix. The summation of the complex amplitudes is revealed when the matrix is properly split (as was done with the intensity generic matrix in the treatment of incoherence):

$$\mathbf{T}_{0/(N+1)} = \begin{bmatrix} T_{11} & T_{12} \\ T_{21} & T_{22} \end{bmatrix} = \mathbf{T}_{0/m}\mathbf{P}_{m}\mathbf{T}_{m/(N+1)}, \tag{17}$$

The complex-amplitude reflection and transmission coefficients of the system are given by the elements of the coherent generic transfer matrix as

$$r_{0,N+1} = \frac{T_{21}}{T_{11}} = r_{0,m} + \frac{t_{0,m}t_{m,0}r_{m,N+1}\exp[-2(\sigma/c)k_m d_m]}{1 - r_{m,0}r_{m,N+1}\exp[-2(\sigma/c)k_m d_m]}, \tag{18}$$

$$t_{0,N+1} = \frac{1}{T_{11}} = t_{0,m}\frac{t_{m,N+1}\exp[-(\sigma/c)k_m d_m]}{1 - r_{m,0}r_{m,N+1}\exp[-2(\sigma/c)k_m d_m]}. \tag{19}$$

Equations (18) and (19) represent the summation of the geometrical series of the field amplitudes, as expected. When the reflection and the transmission coefficients in the right-hand parts of Eqs. (18) and (19) are replaced with their absolute squares, Eqs. (15) and (16) are obtained corresponding to the treatment of incoherence without the use of intensity matrices (this approach was followed in Ref. 14 and is adequate for an arbitrary thin-solid-film multilayer structure on one side of a single thick substrate). Equations (15) and (16) can be seen to be the results of spectral averaging performed taking the integral of the coherent reflectance or transmittance over the spectral window of the polychromatic source.[3]

The splitting of the matrices in both cases [Eqs. (14) and (17)] enabled the representation of the multiple reflections inside the thick substrate as well as the comparison with the Airy summation formulas

found in the literature for a film on a substrate.[15] Although the matrix method may not straightforwardly reveal the multiple reflections inside the multilayer, it retains its simplicity in contrast to the summation formulas,[2,3,15] which become (analytically) cumbersome even for few layers on a substrate.

The advantage of the generic intensity matrix is that its application to multilayers with an incoherent layer in arbitrary position is quite easy. The problem of multilayer structures with more than one incoherent layer[20–27] could also be dealt with in cases such as that with a Fabry–Perot resonator or a beam splitter. As an example we can consider the case of a structure with N layers: medium 0 (semi-infinite)/coherent layers from the first to the $(m-1)$th layer/mth layer incoherent/coherent layers from the $(m+1)$th to the $(j-1)$th layer/jth layer incoherent/coherent layers from the $(j+1)$th to the Nth layer/medium $N+1$ (semi-infinite). The intensity transfer matrix of this system is then

$$\mathbf{T}^{\text{incoh}}_{0/(N+1)} = \mathbf{T}^{\text{int}}_{0/m}\mathbf{P}^{\text{int}}_{m}\mathbf{T}^{\text{int}}_{m/j}\mathbf{P}^{\text{int}}_{j}\mathbf{T}^{\text{int}}_{j/(N+1)}. \tag{20}$$

Prior to the partition of the multilayer in groups of coherent or partially coherent piles and the formation of the corresponding intensity matrices of the groups, each layer is defined in the computation algorithm by its transfer matrix $\mathbf{P}_{m-1}\mathbf{D}^{-1}_{m-1}\mathbf{D}_{m}$ [from Eqs. (1), (2), and (10)]:

$$\frac{1}{t_{m-1,m}}\begin{bmatrix} \Delta_{11}\exp(i\delta_{m-1}) & -\Delta_{12}r_{m,m-1}\exp(i\delta_{m-1}) \\ \Delta_{21}r_{m-1,m}\exp(-i\delta_{m-1}) & (\Delta_{22}t_{m-1,m}t_{m,m-1}-\Delta'_{22}r_{m-1,m}r_{m,m-1})\exp(-i\delta_{m-1}) \end{bmatrix}. \tag{21}$$

When the layer is coherent, the Δ factors become equal to unity ($\Delta_{ij}=\Delta'_{22}=1$), whereas in the case of a layer with a rough side the Δ factors introduce partial coherence ($\Delta_{11}=1/\gamma$, $\Delta_{12}=\beta/\gamma$, $\Delta_{21}=\alpha/\gamma$, $\Delta_{22}=\gamma$, $\Delta'_{22}=\alpha\beta/\gamma$).

The refractive index and the thickness appearing in the phase-thickness parameters, δ_{m-1}, of each layer, should also be defined in the algorithm. The influence of a ($Z=1000$ Å) rough surface or interface is illustrated for a SiC–Si structure in Fig. 2. Two sets of reflectivity spectra were calculated for a 2-μm-thick SiC layer on a thick 300-μm Si substrate, thus introducing partial coherency in the generic matrix. The set of spectra with the high average reflectivity level were calculated assuming the Si substrate to be finite incoherent, whereas for the low-level set the semi-infinite substrate approximation was applied. The spectra corresponding to absence of roughness at both the surface and the interface are displayed in dotted–dashed curves for both sets. The introduction of surface roughness (dotted curves in both sets) leads to a reduction of contrast in the interference-fringe pattern, but the main feature is the lowering of the average reflectivity level at high frequencies. When the 1000 Å roughness is introduced in the interface (solid curves) rather than in the surface, the modification is quite different and easy to distinguish: The influence of interface roughness grows with wave number as well, but instead of lowering the average reflectivity level, it leads to a more severe reduction of contrast in the interference-fringe pattern. When both the surface and the interface exhibit the same amount of roughness (dashed curves), a combination of their characteristic features, that is, the lowering of the average level and the reduction in contrast, respectively, is apparent. However, the difference in the reflectivity level observed between the two sets of spectra results from the average elevation of reflectivity when the Si substrate is considered to be finite and incoherent. This elevation is eliminated in the region of strong lattice absorption, near 800 cm^{-1}, where light is prevented from reaching the backside of the substrate (Si–air interface).

In Fig. 3 the spectrum of Fig. 2 corresponding to a 2-μm SiC layer on a semi-infinite Si substrate exhibiting a 1000Å rough interface is compared with the spectrum of a bulk SiC calculated without roughness (thin and thick solid curves, respectively). It can be seen that the reflectivity of a SiC–Si structure exhibiting a rough interface approaches the reflectivity of bulk SiC at high wave numbers. The influence of a rough surface ($Z=1000$ Å) is also shown in compar-

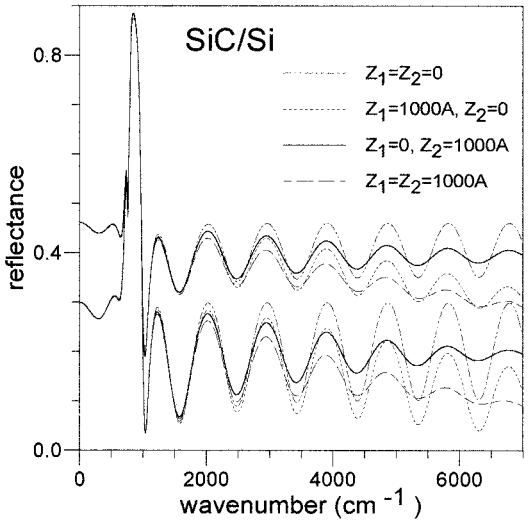

Fig. 2. Influence of a rough surface or interface ($Z=1000$ Å). Two sets of calculated reflectivity spectra for a 2-μm-thick SiC layer on a thick 300-μm Si substrate, introducing partial coherency in the generic matrix. The set of spectra with the high average reflectivity level were calculated assuming the Si substrate to be finite incoherent, whereas for the low-level set the semi-infinite substrate approximation was applied.

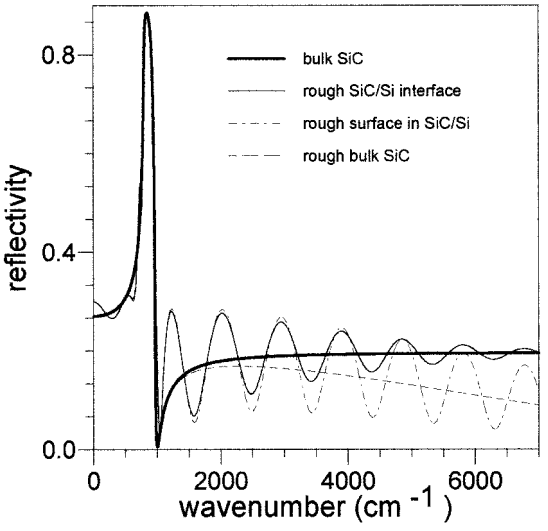

Fig. 3. Comparison of the spectrum of bulk SiC with the spectrum of Fig. 2 corresponding to a 2-μm SiC layer on a semi-infinite Si substrate exhibiting a 1000Å rough interface (thick and thin solid curves, respectively). The influence of a rough surface (Z = 1000Å) is also shown in comparison (dashed and dotted–dashed curves).

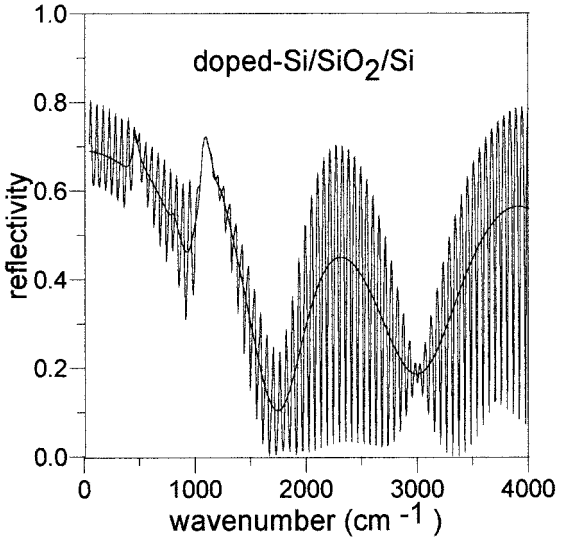

Fig. 4. Calculated reflectance spectra of a doped Si–SiO_2–thick-Si structure with the generic matrix formulation (d_{Si} = 0.08 μm, d_{SiO2} = 1.6 μm, d_{Si} = 850 μm). The calculations were performed considering either a coherent substrate of finite thickness (spectrum with narrow oscillations) or an incoherent one (smooth spectrum).

ison (dashed and dotted–dashed curves). The spectrum of bulk SiC exhibiting surface roughness is in fact the average of the corresponding fringe pattern of a SiC–Si structure with an ideal SiC–Si interface and 1000Å surface roughness. Figure 3 justifies the features discussed for a film on a substrate in Fig. 2. Interface roughness destroys interference, maintaining the average reflectivity to the level of the bulk, whereas surface roughness lowers the average reflectivity, since it prevents greater amounts of light from entering the sample as the wave number increases.

In the lattice vibration region of the reflectivity spectra of Fig. 3 [ω_{TO} = 796.5 cm^{-1}, γ_{TO} = 20 cm^{-1}, $\Delta\epsilon$ = 3.3, ϵ_∞ = 6.7; see Eq. (22)] between 790 and 870 cm^{-1} the SiC film becomes opaque and its spectrum overlaps the spectrum of bulk SiC. The SiC–Si interface, either rough or smooth, cannot contribute to reflectivity, and only the existence of surface roughness could be revealed, in this region, after plotting in a different scale.

The effect of a thick layer, either coherent or incoherent, is illustrated with the calculated spectra of Fig. 4. The generic system transfer matrix was used for the calculation of reflectance of an air–doped-Si–SiO_2–Si–air structure. Structures of buried amorphous SiO_2 in Si, easily obtained by oxygen ion implantation or wafer bonding, are of great technological importance.[28–31] The top Si layer was assumed to be homogeneously doped and to have a free-carrier volume concentration of 2.5×10^{20} cm^{-3}, and a thickness of 0.08 μm. The buried insulating SiO_2 layer was 1.6 μm thick, had a lower refractive index (ϵ_∞ = 2.14 compared with the ~11.7 value of Si at 9000 cm^{-1}), and exhibited resonance at 455, 800, 1065, and 1200 cm^{-1}. The thick (850-μm) Si substrate lead to narrow oscillations in the spectrum when the coherent formulation was used. Thick-film interference is suppressed when the substrate is considered to be incoherent, leading to a smoothing of the spectrum as can be seen in Fig. 4. The shape of the smooth spectrum is independent of the substrate thickness when the substrate is transparent [k_N = 0 in Eq. (16)]. In this case the incoherent substrate propagation matrix becomes equal to the identity matrix.

In the region of the strong atomic vibration absorption of SiO_2 (1065 cm^{-1}) in Fig. 4 the narrow (thick-film) oscillations vanish, indicating that light does not reach the substrate. For lower frequencies, however, the levels of light absorption drop and thick-film oscillations appear again. Their amplitude is drastically reduced compared with that of the transparent region above 2000 cm^{-1}, on account of the absorption of light associated with free-carrier excitations. Light thus reaches the substrate in this spectral region. The above discussion is also justified by the values of the transmissivity of light in the substrate calculated assuming a semi-infinite substrate (10% in the low-frequency limit as well as 1% and 0.4% in the region of the two strongest lattice resonances).

3. Refractive-Index Profiling in the Infrared Wavelength Region

The refractive-index profile assumed to simulate the one-dimensional inhomogeneity of a sample under investigation can be partitioned into an unlimited number of uniform layers. Each layer is represented by its transfer matrix of Eq. (21) and defined by its thickness, d, and by its complex refractive index, $\tilde{n}$, or by its complex permittivity, $\tilde{\epsilon}$ (the square of

the complex refractive index). In the general case the complex permittivity of each layer in the infrared is given as a function of wave number ω as[8,32]

$$\tilde{\epsilon} = \sum_j \frac{\Delta\epsilon_j(\omega_{TOj})^2}{\omega_{TOj}^2 - \omega^2 - i\gamma_j\omega} - \frac{\omega_p^2\epsilon_\infty}{\omega^2 + i\gamma_j\omega} + \epsilon_\infty. \quad (22)$$

The parameters should vary from layer to layer (in order to simulate the depth variation of the refractive index).

The first term, which results from the interaction of ions or atoms of the solid with the electromagnetic field is the sum of the contributions to the dispersion. It is the so-called lattice dispersion, and the atomic vibrational parameters of ω_{TO}, γ, and $\Delta\epsilon$ (TO frequency, damping constant, and oscillator strength, respectively) have their usual spectroscopic meaning.[8,32] The second term is due to intraband carrier transitions[8,33] (ω_p, plasma frequency; γ_p, free-carrier damping) within the conduction or valence band, whereas, the third term, ϵ_∞, is due to bound electrons (its weak dispersion in the infrared usually represented by a Sellmeir or Cauchy equation[1,5]).

The way a depth variation of a parameter is encountered in the matrix equations is illustrated below for an implantation doped Si wafer with a Gaussian depth distribution[8] of free carriers (with a standard deviation ΔR).

The carrier profile is directly partitioned into $2\kappa(\Delta R)/\delta x$ homogeneous layers of equal thickness $\delta x(=\Delta R/10)$ with the carrier concentration N_{Cj} in each layer given as

$$N_{cj} = N_{c,\max}\exp[(-1/2)\{[-\kappa\Delta R + j\delta x]/\Delta R\}^2], \quad (23)$$

where $N_{c,\max}$ is the peak of the concentration profile and j is the layer counter. Convergence tests show that by truncation of the Gaussian at 2κ standard deviations, the resulting steps in the refractive-index profile have a negligible influence on the calculated spectrum (less than the experimental accuracy of 0.003 for the difference in absolute reflectance values) when κ is set equal to 4 or in some cases even 3. The depth dependence of the dielectric function is related to the carrier concentration dependence of the plasma frequency given as[8]

$$\omega_{pj}^2 = \frac{4\pi N_{cj}e^2}{m^*}, \quad (24)$$

where $m^*(\approx 0.3m_e)$ is the conductivity effective mass of electrons in Si.

Given the depth dependence of $N_c(x)$, the optical constants can thus be computed for each layer comprising the carrier profile, as follows:

a. The complex dielectric function $\tilde{\epsilon} = \epsilon' + i\epsilon'' = (n - ik)^2$ is calculated for each layer and written in terms of its real and imaginary parts. For the j layer this yields

$$\epsilon'_{cj} = n_j^2 - k_j^2 = \epsilon_\infty - \frac{\omega_{pj}^2\epsilon_\infty}{\omega^2 + \gamma_p^2}, \quad (25a)$$

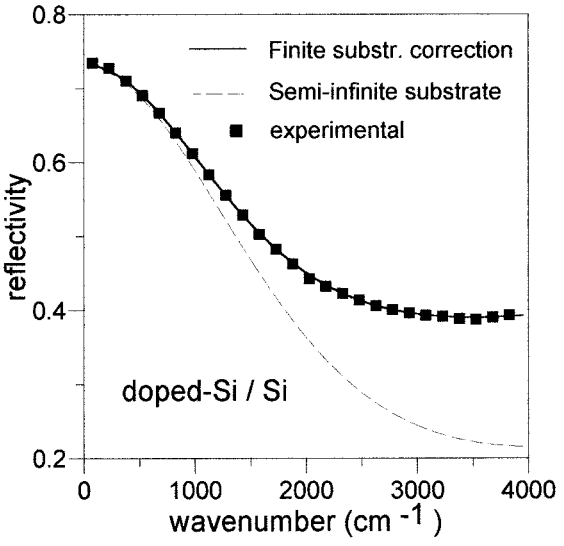

Fig. 5. Experimental and calculated reflectance of a doped-Si–Si structure (70 keV, 6×10^{15} As^+cm^{-2}, 0.5 h annealed at 950 °C) with application of either the incoherent finite-substrate correction or the semi-infinite substrate approximation. The 0.286-μm-thick inhomogeneous doped Si region was partitioned into 80 sampling layers simulating two half-joined Gaussians (R_P = 3800Å, ΔR_1 = 95Å, ΔR_2 = 620Å).

$$\epsilon''_{cj} = 2n_jk_j = \frac{\gamma_p\omega_{pj}^2\epsilon_\infty}{\omega(\omega^2 + \gamma_p^2)}. \quad (25b)$$

b. Equations (25) are solved for the refractive index n_j and extinction coefficient k_j,

$$n_j = \{\tfrac{1}{2}[\epsilon'_j + (\epsilon'^2_j + \epsilon''^2_j)^{1/2}]\}^{1/2},$$
$$k_j = \{\tfrac{1}{2}[-\epsilon'_j + (\epsilon'^2_j + \epsilon''^2_j)^{1/2}]\}^{1/2}. \quad (26)$$

These optical parameters and the thickness, $d_j = \delta x$, of each layer are then introduced into the multilayer matrix equations to compute the reflectance as a function of frequency.

The model also includes as adjustable parameters the rms heights Z_i, of surface and/or interface irregularities, which can be viewed as macroscopic roughness. Z_i is initially set to zero and is allowed to be fitted only when the fit quality does not improve (after several models have been tried).

4. Applications

A. Inhomogeneous Layer on a Thick Substrate

An example of simulation of an inhomogeneous ion-implanted area that uses multilayer modeling is illustrated in Figs. 5 and 6. Figure 5 illustrates experimental and calculated reflectance spectra of a doped Si slab. The thickness of the slab is 200 μm, whereas that for the doped region is 0.286 μm. The doped region was formed after 70 keV, 6×10^{15} As^+cm^{-2} implantation followed by annealing at 950 °C for 1/2 h. The free-carrier concentration depth profile in the doped region was simulated by use of two half-joined Gaussians, each one parti-

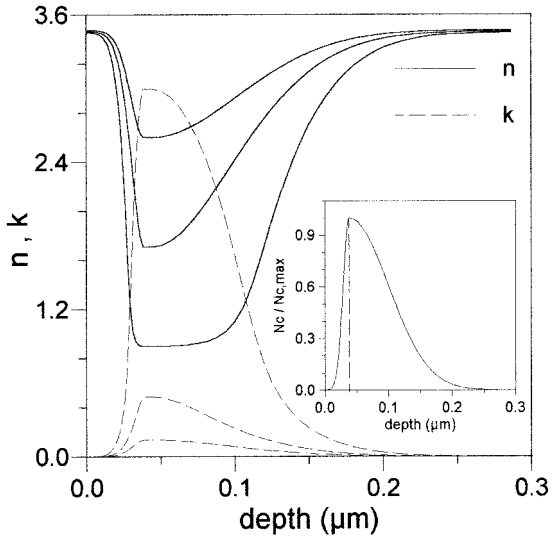

Fig. 6. Depth profiles of the real and the imaginary parts of the refractive index, n and k, corresponding to the free-carrier asymmetric-Gaussian profile in the doped Si–Si structure of Fig. 5 calculated at $\sigma = 2000$, 3000, and 4000 cm^{-1}. As σ increases, the contribution of the free-carrier plasma dispersion diminishes and the magnitudes of the dip in n and the peak in k decrease. The inset exhibits two half-joined Gaussians modeling the carrier concentration depth profile.

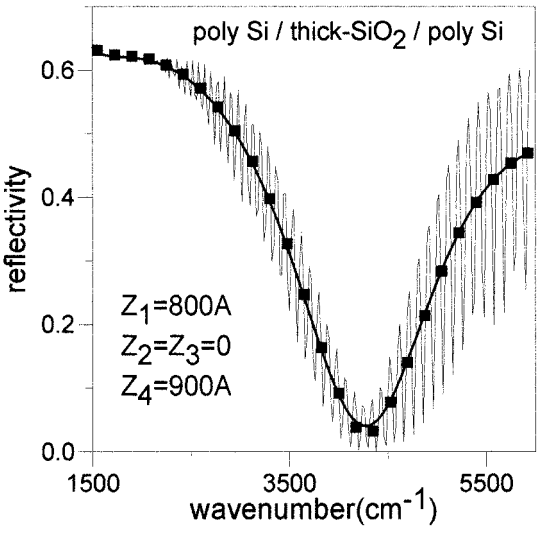

Fig. 7. Experimental and calculated reflectance spectra of a 370-μm-thick SiO_2 layer between two thin poly-Si layers with thickness 0.34 and 0.35 μm, respectively. The best-fit reflectivity (thick solid curve) was calculated with the incoherent finite-substrate formalism for a thick intermediate layer. Roughness at both the front and the rear Si surfaces was detected: 800Å and 900Å, respectively. The thin solid curve designating a dense fringe pattern was calculated assuming the oxide substrate to be coherent, for comparison.

tioned to 40 layers (see inset in Fig. 6). For the surface-side half-Gaussian a standard deviation of $\Delta R_1 = 95$Å was chosen, whereas for the bottom the standard deviation chosen was $\Delta R_2 = 620$Å. The maximum of the free-carrier concentration (where the two half-Gaussians join) was found to be approximately 3×10^{20} cm^{-3}. The semi-infinite substrate approximation failed to give a fit at high frequencies. An appreciable fit was obtained only when the finite substrate correction was used (Fig. 5). The translation of the assumed free-carrier concentration depth profile to the corresponding depth profiles of the optical constants (the real and the imaginary parts of the refractive index) is illustrated in Fig. 6 for three different frequencies (2000, 3000, and 4000 cm^{-1}). The effects of dispersion are apparent: The higher the frequency, the lower the distortion caused by the free carriers to the refractive index of Si.

B. Thick Incoherent Substrate between Partially Coherent Layers

Figure 7 illustrates experimental data (squares) and the best fit (thick solid curves) for a sample with an incoherent substrate between partially coherent layers (air–Si–thick SiO_2–Si–air). The three-layer structure was formed by low-pressure chemical vapor deposition (LPCVD) of poly Si on both sides of a thick SiO_2 substrate. The LPCVD process involved decomposition of silane gas at 630 °C. Fourier-transform infrared (FTIR) analysis revealed the thickness values of the three layers to be $d_1 = 0.34$ μm, $d_2 = 370$ μm, and $d_3 = 0.35$ μm. The SiO_2 layer (layer 2) was considered to be incoherent, and the intensity matrices were used. If the SiO_2 substrate was considered to be coherent, a dense fringe pattern would have occurred. This is illustrated by the thin solid curve in Fig. 7 with a plotting step of 20 cm^{-1}. In the low-frequency portion of the illustration in Fig. 7 it is seen that the two spectra are coincident. This is expected, since at low frequencies the substrate exhibits strong absorption, preventing light from reaching the back SiO_2–Si interface.

The roughness parameters of the front and the rear Si–SiO_2 interfaces (Z_2 and Z_3, respectively) were found to be below the 100Å low detectable limit of FTIR spectroscopy for this sample. The spectra were taken at Aristotle University of Thessaloniki with a Bruker IFS113v spectrophotometer. The roughnesses at the two surfaces of the poly-Si layers were determined to be $Z_1 = 800$Å for the front Si and $Z_4 = 900$Å for the rear Si surface. It can be seen that the effects of roughness become important at high frequencies at which the wavelength of radiation cannot be considered too large compared with the surface or interface inhomogeneities.

With the best-fit layer thickness and refractive-index values for the experimental data of Fig. 7 a set of calculated spectra was created, illustrated in Fig. 8. These calculated spectra exhibit how the same amount of roughness can affect FTIR spectra in a different way depending on which interface is rough. Circles represent the case of completely smooth surface interfaces. Diamonds and squares represent the cases of a 900Å roughness in the front surface and the front Si–SiO_2 interface, respectively. The effects of either the back SiO_2–Si interface or the backsur-

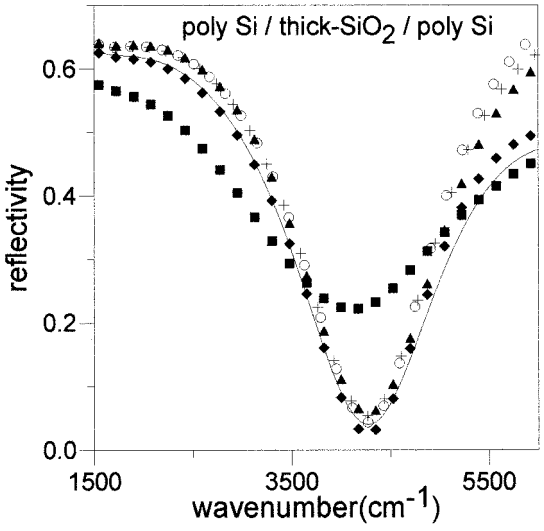

Fig. 8. Combined action of incoherence and partial coherence within a multilayer. Symbols represent calculated reflectance spectra with refractive index and thickness parameters of the poly-Si–thick-SiO_2–poly-Si structure of Fig. 7. Only one interface is considered to be rough (Z = 900 Å) at a time. Circles, no roughness; diamonds, surface rough; squares, front Si–SiO_2 interface rough; crosses, rear Si–SiO_2 interface rough; triangles, backsurface rough. The solid curve is the best-fit curve of Fig. 7: both poly-Si surfaces rough, Z_1 = 800 Å and Z_4 = 900 Å.

face (Si–air interface) exhibiting roughness of 900Å are illustrated by the crosses and the triangles, respectively. The solid curve represents the combined action of the two Si surfaces being rough. It is actually the best-fit curve of Fig. 7. In such a structure with an incoherent layer sandwiched between coherent ones, features similar to those in Fig. 2 are observable as well regarding the influence of the Z parameters.

5. Conclusion

The matrix method for the analysis of the optical response of coherent multilayers has been generalized to take into account partially coherent and incoherent reflected or transmitted light. This approach is also integrated to include models for refractive-index depth profiling. Its applicability was demonstrated concerning the optical characterization of ion-implanted materials as well as multilayers with a thick substrate in an arbitrary position within their structure and multilayers of conducting or insulating layers with rough surface and interfaces.

This research was financially supported by the Greek General Secretariat of Research and Technology, Ministry of Development, under project PENED96/1424.

References

1. M. Born and E. Wolf, *Principles of Optics* (MacMillan, New York, 1964), p. 254.
2. O. S. Heavens, *Optical Properties of Thin Films* (Dover, New York, 1965), p. 69.
3. P. Yeh, *Optical Waves in Layered Media* (Wiley, New York, 1988), p. 102.
4. Z. Knittl, *Optics of Thin Films* (Wiley, London, 1976), p. 41.
5. G. K. Hubler, P. R. Malmberg, C. N. Waddell, W. G. Spitzer, and J. E. Fredrickson, in *Ion Implantation for Materials Processing*, F. A. Smidt, ed. (Noyes Data, Park Ridge, N.J., 1983), p. 195–218.
6. W. Tennant and J. Cape, "Study of the dielectric function of PbSnTe epitaxial film by far-infrared reflectivity," Phys. Rev. B **13,** 2540–2547 (1976).
7. C. C. Katsidis, D. I. Siapkas, W. Skorupa, N. Hatzopoulos, and D. Panknin, *Proceedings of the 10th International Conference on Ion Implantation Technology* (Elsevier, Amsterdam, 1995), p. 959–962.
8. C. C. Katsidis and D. I. Siapkas, in *Proceedings of NATO ASI on Application of Particle and Laser Beams in Materials Technology*, P. Misaelides, ed. (Kluwer Academic, Dordrecht, 1995), p. 603–612.
9. C. C. Katsidis, D. I. Siapkas, D. Panknin, N. Hatzopoulos, and W. Skorupa, "Optical characterization of doped Simox structures using FTIR spectroscopy," Microelectron. Eng. **28,** 439–442 (1995).
10. N. Hatzopoulos, D. I. Siapkas, and P. L. F. Hemment, "Oxide growth, refractive index, and composition depth profiles of structures formed by 2 MeV oxygen implantation into silicon," J. Appl. Phys. **77,** 577–586 (1995).
11. D. I. Siapkas, N. Hatzopoulos, C. C. Katsidis, T. Zorba, C. L. Mitsas, and P. L. F. Hemment, "Structural and compositional characterization of high energy separation by implantation of oxygen structures using infrared spectroscopy," J. Electrochem. Soc. **143,** 3019–3032 (1996).
12. N. Hatzopoulos, D. I. Siapkas, P. L. F. Hemment, and W. Skorupa, "Formation and characterization of novel Si/SiO2 multilayer structures by oxygen ion implantation into silicon," J. Appl. Phys. **80,** 4960–4970 (1996).
13. N. Hatzopoulos, D. I. Siapkas, and P. L. F. Hemment, "Optical investigation of structures formed by 2MeV oxygen implantation into silicon," Thin Solid Films **289,** 90–94 (1996).
14. C. L. Mitsas and D. I. Siapkas, "Generalized matrix method for analysis of coherent and incoherent reflectance and transmittance of multiplayer structures with rough surfaces, interfaces, and finite substrates," Appl. Opt. **34,** 1678–1683 (1995).
15. G. Lubberts, B. C. Burkey, F. Moser, and E. A. Trabka, "Optical properties of phosphorous-doped polycrystalline silicon layers," J. Appl. Phys. **52,** 6870–6878 (1981).
16. I. Fillinski, "The effects of sample imperfections on optical spectra," Phys. Status Solidi **49,** 577–588 (1972).
17. J. Szczyrbowski and A. Czapla, "Optical absorption in d.c. sputtered InAs films," Thin Solid Films **46,** 127–137 (1977).
18. J. Pawlikovski, "Comments on the determination of the absorption coefficient of thin semiconductor films," Thin Solid Films **127,** 29–38 (1985).
19. H. E. Bennett, and J. O. Porteus, "Relation between surface roughness and specular reflectance at normal incidence," J. Opt. Soc. Am. **51,** 123–129 (1961).
20. A. Tikhonravov, M. Trubetskov, B. Sullivan, and J. Dobrowolski, "Influence of small inhomogeneities on the spectral characteristics of single thin films," Appl. Opt. **36,** 7188–7198 (1997).
21. A. Roos, M. Bergquist, and C. Ribbing, "Determination of the SiO_2/Si interface roughness by diffuse reflectance measurements," Appl. Opt. **27,** 4660–4663 (1988).
22. A. Roos, M. Bergquist, and C. Ribbing, "Optical scattering from oxidized metals. 1. Model formulation and properties," Appl. Opt. **28,** 1360–1364 (1989).
23. A. M. Dioffo, "Étude théorique des caractéristiques optiques

d'un système de lames diélectriques," Rev. Opt. **47,** 49–68 (1968).
24. C. J. Gabriel and A. Nedoluha, "Transmittance and reflectance of systems of thin and thick layers," Opt. Acta **18,** 415–423 (1971).
25. R. Z. Vitlina and G. I. Surdutovich, "A 'blurred film' model in polarized light reflectometry for characterization of thick films and surface layers," J. Phys. D. Appl. Phys. **34,** 2593–2598 (2001).
26. R. Swanepoel, "Determination of the thickness and optical constants of amorphous silicon," J. Phys. E **16,** 1214–1222 (1983).
27. C. C. Katsidis, D. I. Siapkas, A. K. Robinson, and P. L. F. Hemment, "Formation of conducting and insulating layered structures in Si by ion implantation: process control using FTIR spectroscopy," J. Electrochem. Soc. **148,** G704–G716 (2001).
28. A. K. Robinson, K. J. Reeson, and P. L. F. Hemment, "Redistribution and electrical activation of implanted arsenic in silicon on insulator substrates formed by oxygen ion implantation," J. Appl. Phys. **68,** 4340–4342 (1990).
29. Z. Wenhua, L. Chenglu, S. Zuoyu, Z. Shichang, P. L. F. Hemment, and A. Nejim, "Electrical characterization of thin film Simox structures," Nucl. Instrum. Meth. B **74,** 218–221 (1993).
30. J. Stoemenos, A. Carcia, B. Aspar, and J. Margail, "Silicon on insulator obtained by high dose oxygen implantation, microstructure, and formation mechanism," J. Electrochem. Soc. **142,** 1248–1259 (1995).
31. N. Hatzopoulos, W. Skorupa, and D. Siapkas, "Double Simox structures formed by sequential high energy oxygen implantation into silicon," J. Electrochem. Soc. **147,** 354–362 (2000).
32. D. I. Siapkas, D. B. Kushev, N. N. Zheleva, J. Siapkas, and I. Lelidis, "Optical constants of tin-telluride determined from infrared interference spectra," Infrared Phys. **31,** 425–433 (1991).
33. K. Krishnan, P. J. Stout, and M. Watanabe, *Practical Fourier Transform Infrared Spectroscopy* (Academic, New York, 1990), p. 294.